Figure S1

A

599 RNase One+V1

599 RNase One+V1 + ProK

NOP2

1kb

145 RNase One+V1

145 RNase One+V1 + ProK

GNB3

1kb

69 RNase One+V1

69 RNase One+V1 + ProK

RUSF1

2kb

B

Structure Score

-1

-5

-50bp   Alu   +50bp

n=82134

C

Fraction mismatches

0.2

0.1
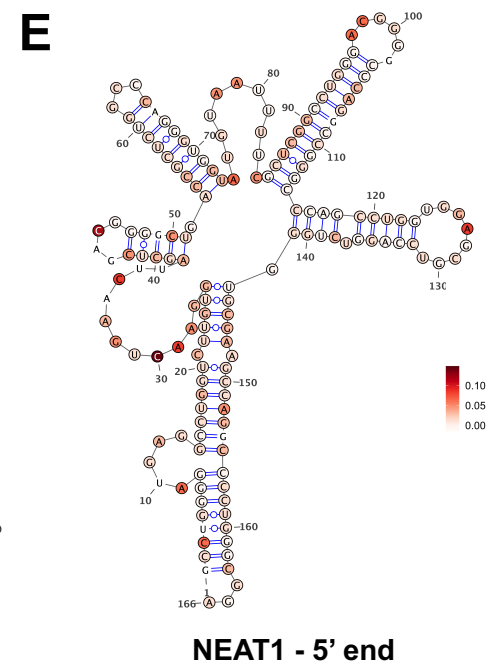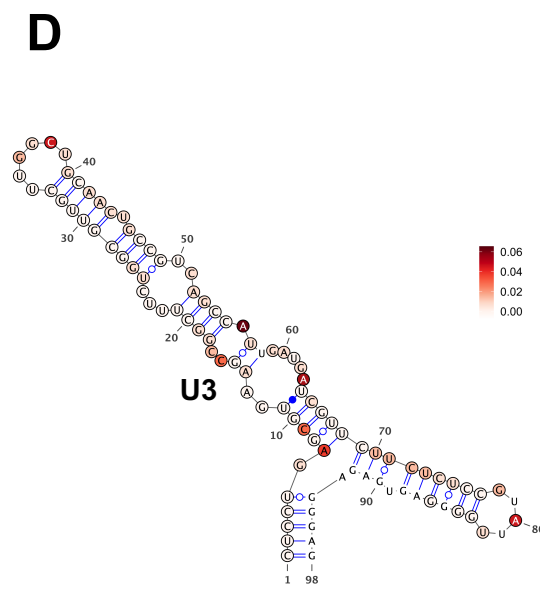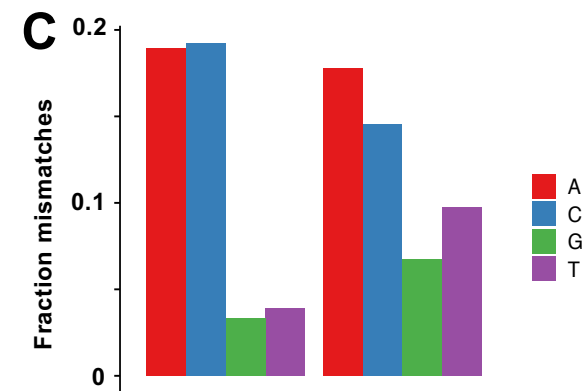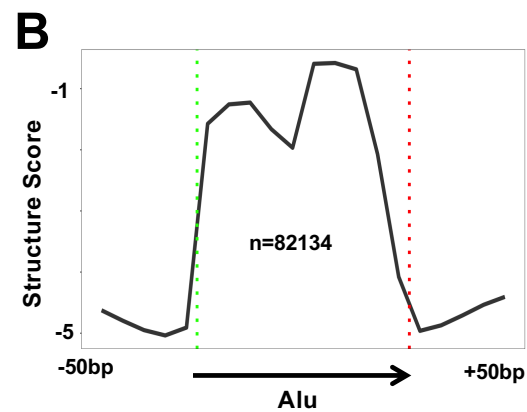
0

A
C
G
T

D

U3

E

NEAT1 - 5' end

Figure S1. Related to Figures 1, 2.

A. IGV browser screen shots comparing representative regions for putative protein footprints RNAseOne+V1 resistant reads with regions resistant to RNAses after proteinase K digestion.

B. Metaplot of mean Structure Score from tNet-RNAse-seq at expressed Alu elements (5 base bins). Note that as expected Alu elements are highly structured.

C. Frequency of DMS induced mutations detected by tNET-Mapseq in nascent pol II transcripts from HEK293 cells expressing WT Am^r Rpb1 and the Rpb1 R749H slow mutant. Note highest levels of modification at A and C residues with less modification at U and G (Mustoe et al., 2019) as expected. Low level modification at U and G is informative in structure prediction.

D, E. Predicted structures drawn using VARNA (v3-93) and U3 and the NEAT1 5' end chr11:65,190,783-65,190,949 (Lin et al., 2018) with DMS reactivities in nascent RNA from HEK293 cells expressing WT Am^r Rpb1 indicated in color.
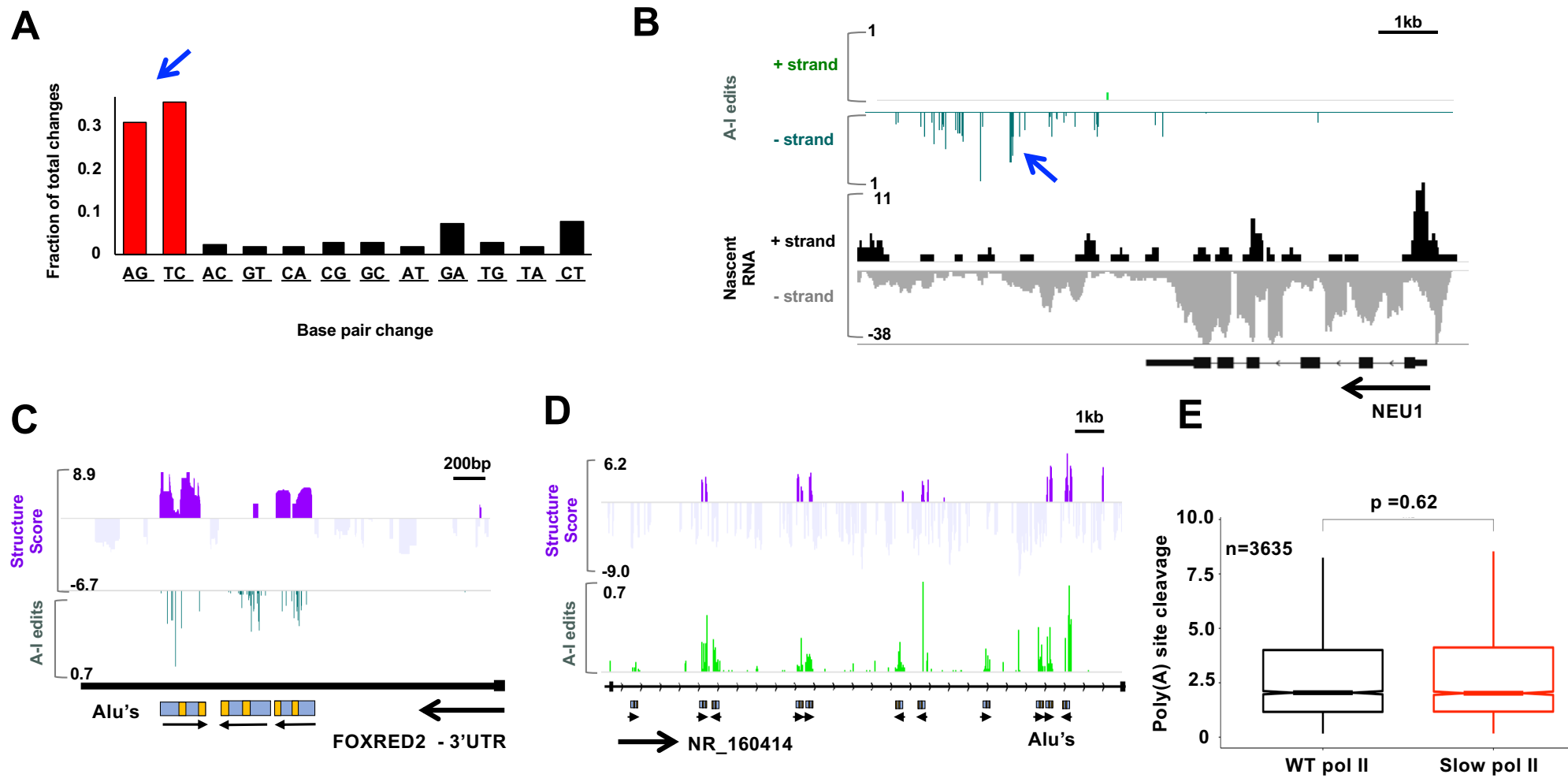
A

B

1kb

A-I edits

+ strand

– strand

1

Nascent RNA

11

+ strand

– strand

–38

NEU1

C

200bp

Structure Score
8.9

–6.7

A-I edits
0.7

Alu's

FOXRED2 - 3'UTR

D

1kb

Structure Score
6.2

–9.0

A-I edits
0.7

NR_160414

Alu's

E

p =0.62

n=3635

Poly(A) site cleavage

10.0

7.5

5.0

2.5

0.0

WT pol II   Slow pol II

Figure S2

Figure S2. Related to Figure 2

 A. Frequency of base substitutions associated with A-I editing in tNET-seq reads in HEK293 expressing WT Am^r Rpb1 determined using Reditools (Picardi and Pesole, 2013) showing the bias toward A-G and T-C substitutions expected for A-I editing.

B. Nascent RNA reads and fraction of A-I editing per base for NEU1. Note extensive editing in 3' flanking region (blue arrow).

C, D. Coincidence of RNA structure score determined by tNET RNAse-seq with A-I editing at inverted Alu elements.

E. Quantitation of unprocessed pre-mRNA transcripts in merged tNET-seq nascent RNA preparations. For each gene the number of uncleaved reads that include the 10 base region from -5 to +5bp relative to the poly(A) cleavage site were normalized by dividing into the number of reads in the region from -1000 to -500bp relative the cleavage site (see Star Methods).
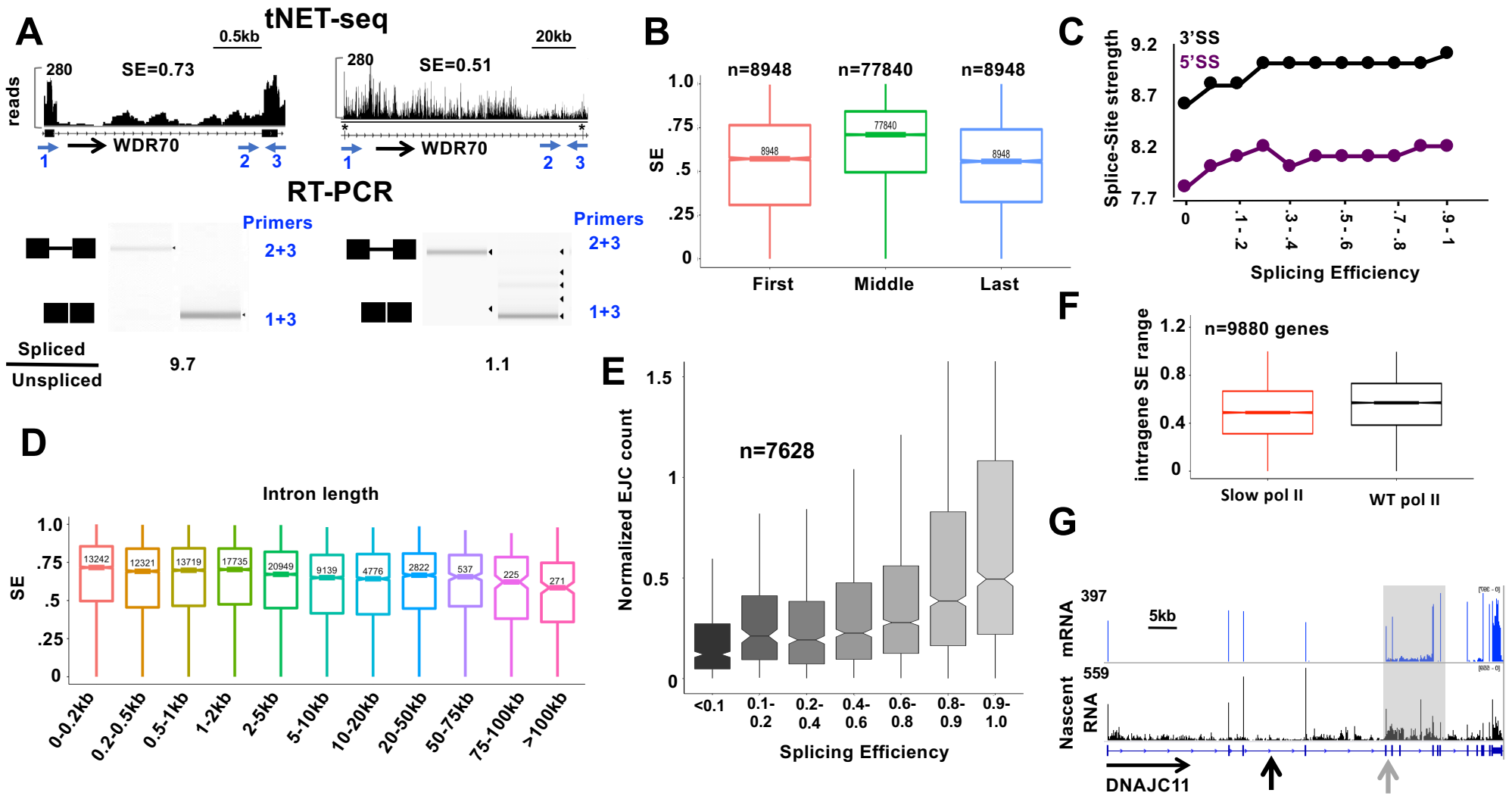
Figure S3

Figure S3. Variation and coordination of co-transcriptional splicing. Related to Figure 3.

A. RT-PCR validation of differential co-transcriptional splicing efficiency (SE) determined from tNET-seq for two introns in WDR70. Immunoprecipitated nascent RNA was random-primed and PCR amplified with indicated primers. Note that RT-PCR confirmed more efficient co-transcriptional splicing of intron 11 (chr5:37,701,206-37,703,115) (left) than intron 9 (chr5:37,604,474-37,699,523) (right, * indicates introns). Concentrations shown below bands calculated using Agilent tape station software.

B. Median SE values calculated from tNET-seq for genes with ≥3 introns show more efficient co-transcriptional splicing of internal introns than terminal introns consistent with previous work (Khodor et al., 2011; Pai et al., 2017; Tilgner et al., 2012).

C. Relation of SE values determined from tNET-seq to splice site strengths calculated by MaxEnt (Yeo and Burge, 2004).

D. Relation of co-transcriptional splicing efficiency (SE) to intron length shows reduced SE for long introns consistent with previous work (Khodor et al., 2011). Genes with ≥3 introns were considered.

E. Co-transcriptional splicing efficiency (SE) correlates with deposition of putative exon junction complexes (EJC's) defined at protein footprints on spliced reads that cover the region (>10 bases) immediately upstream of splice sites as detected by resistance to RNAseI+RNAseVI (see Fig. 1A).

F. The range of SE values for introns within genes having >3 introns in nascent RNA. Median values are 0.49 and 0.57 for cells expressing slow and WT pol II respectively.

G. IGV browser shot of mRNA and nascent RNA-seq (tNET-seq) showing co-transcriptionally well-spliced (black arrow SE=.97) and poorly spliced (gray arrow SE=0.25) introns and clustering of introns (grey box) with coordinated co-transcriptional splicing (SE < 0.4).
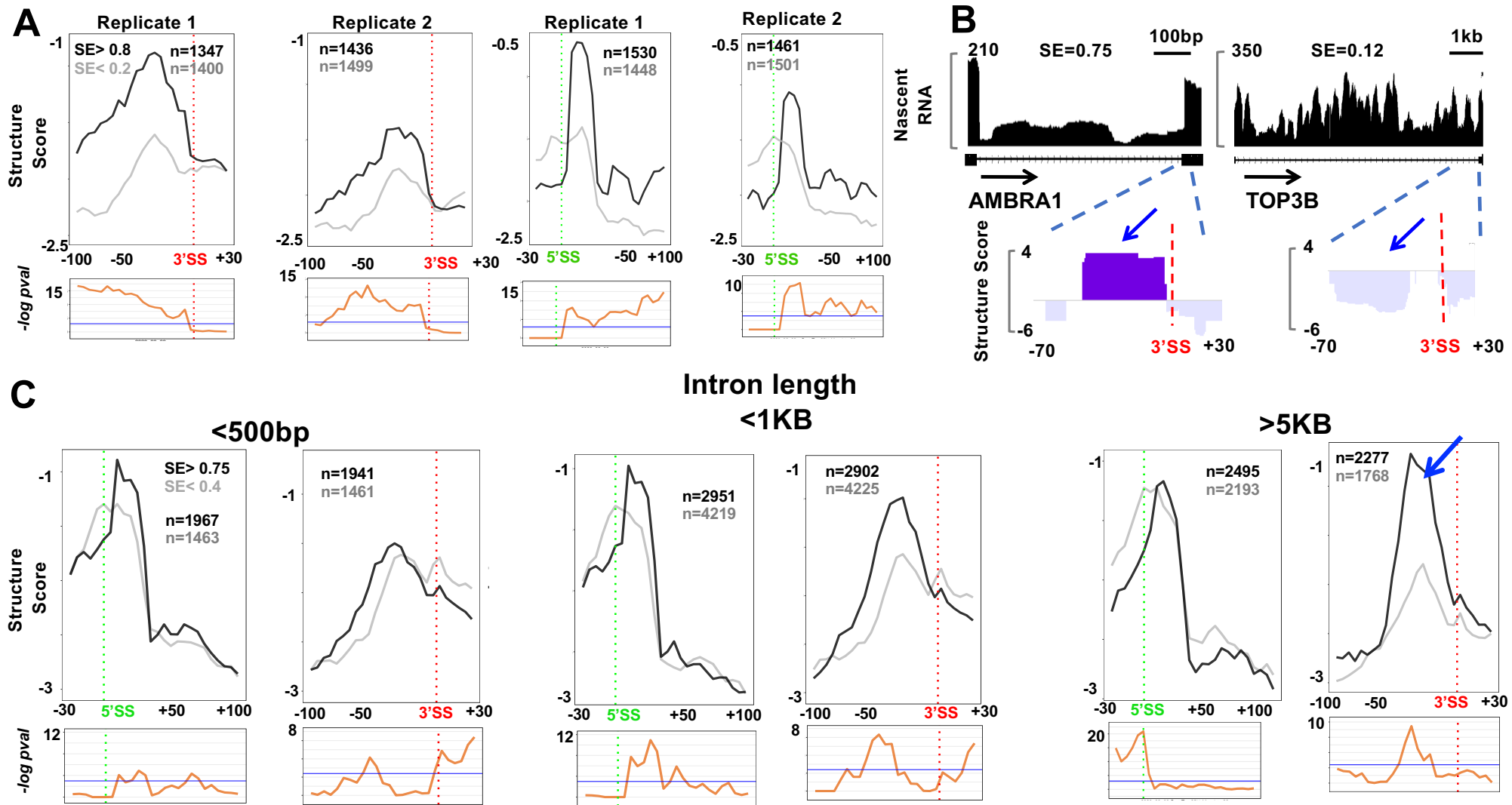
A

Replicate 1
SE> 0.8   n=1347
SE< 0.2   n=1400

Structure Score
-1
-2.5

-log pval
15

Replicate 2
n=1436
n=1400

-1
-2.5

-log pval
15

+30

Replicate 1
n=1530

-0.5

-log pval
15

Replicate 2
n=1461
n=1501

-0.5
-2.5

-log pval
10

B

Nascent RNA

210   SE=0.75   100bp

AMBRA1

350   SE=0.12   1kb

TOP3B

Structure Score
4
-6
-70   3'SS   +30

4
-6
-70   3'SS   +30

C

Intron length

<500bp

SE> 0.75
SE< 0.4

Structure Score

-log pval
12

8

<1KB

-1

-3
-30   5'SS   +50   +100

-1

-3
-50   3'SS   +30

-log pval
12

8

>5KB

n=2277

-log pval
20

Figure S4

Figure S4. Related to Figure 3

A. Metaplots of nascent RNA mean Structure Score across 5' and 3' splice sites (5 base bins) of co-transcriptionally well-spliced (SE> 0.8, black) and poorly spliced (SE < 0.2, gray) introns in two independent replicate experiments. FDR values as in Fig. 3E.

B. Distinct RNA structural motifs (blue arrows) at the 3' SS of introns with high (AMBRA1 chr11:46,568,777-46,569,421) and low (TOP3B chr22:22,330,059-22,336,880) co-transcriptional splicing efficiency, SE. IGV screen shots are shown of Nascent RNA-seq and Structure Score in the region -70 to +30 bases relative to the splice site.

C. Metaplots of nascent RNA Structure Score across 5' and 3' splice sites (5 base bins) of co-transcriptionally well-spliced (SE> 0.75 black) and poorly spliced (SE < 0.4, gray) introns of different lengths. Note that steep 3'SS steps (blue arrows) are most strongly associated with high co-transcriptional splicing of long introns.
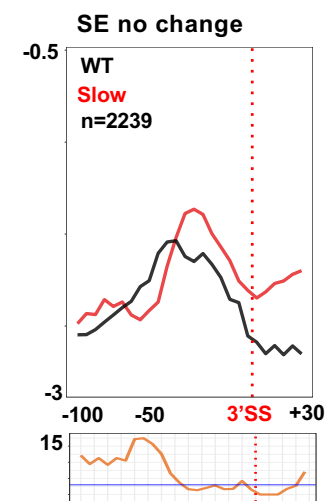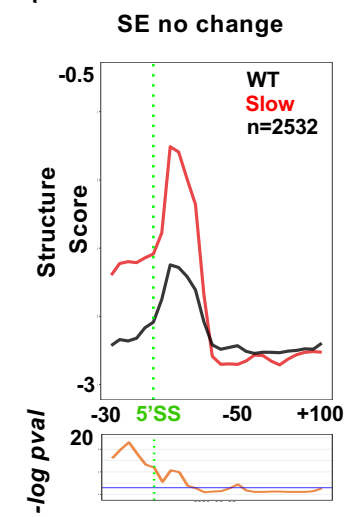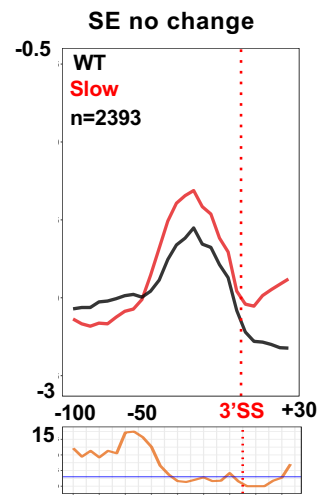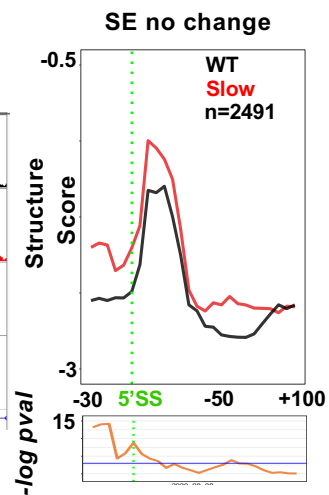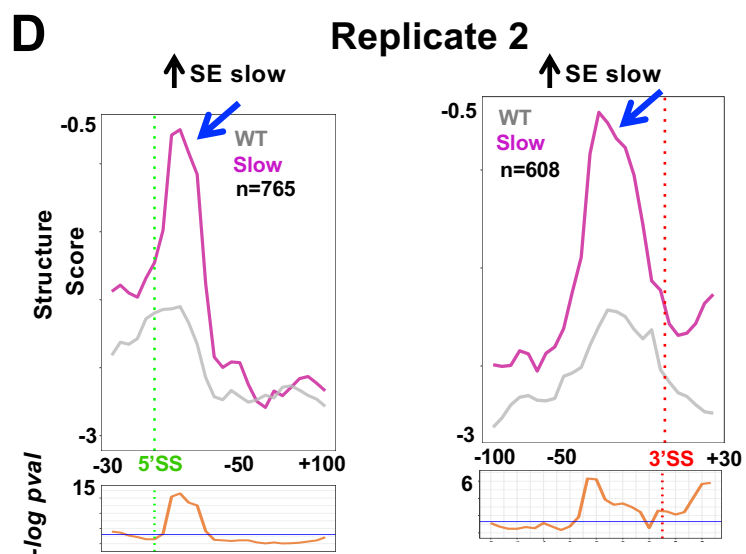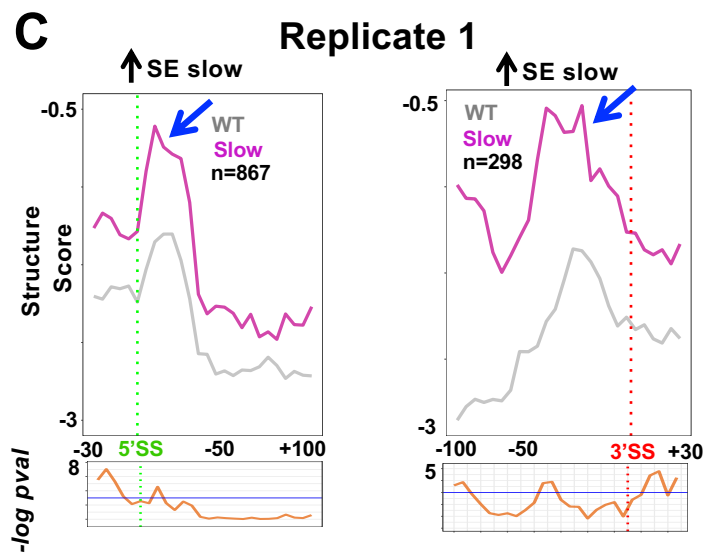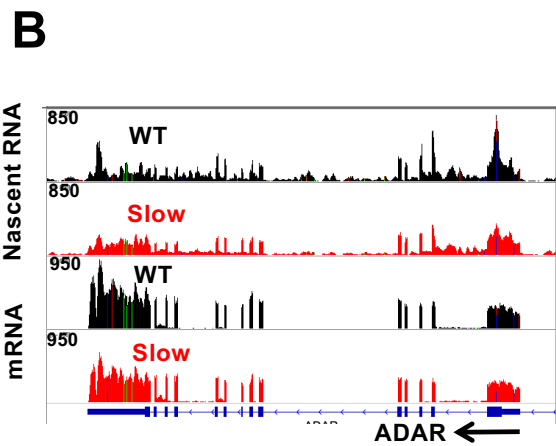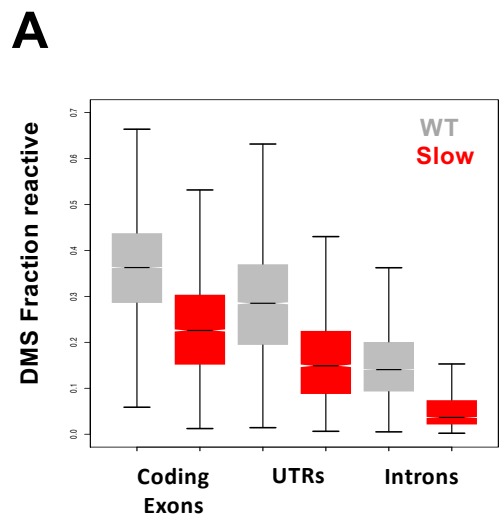
Figure S5

Figure S5. Related to Figure 5.

A. Slow transcription increases nascent RNA structure. DMS reactivity is plotted for coding exons, UTRs and introns in cells expressing WT and slow mutant (R749H) pol II. Note reduced reactivity of all regions in the slow mutant.

B. Slow pol II does not cause over-expression of ADAR1. IGV genome browser screen shots of nascent RNA seq (tNET-seq, top panels) and mRNA (bottom panels) for ADAR in HEK293 Flp-in cells expressing WT and slow pol II.

C, D. Structure Score across the 5' and 3' splice sites in cells expressing WT and slow mutant pol II for introns whose SE is increased by slow transcription (grey and pink) or those that are unaffected (black and red) in two independent replicates. Note the elevated intronic RNA structure and steeper 5' and 3' SS steps at splice sites where co-transcriptional splicing is stimulated by slow transcription (blue arrows).
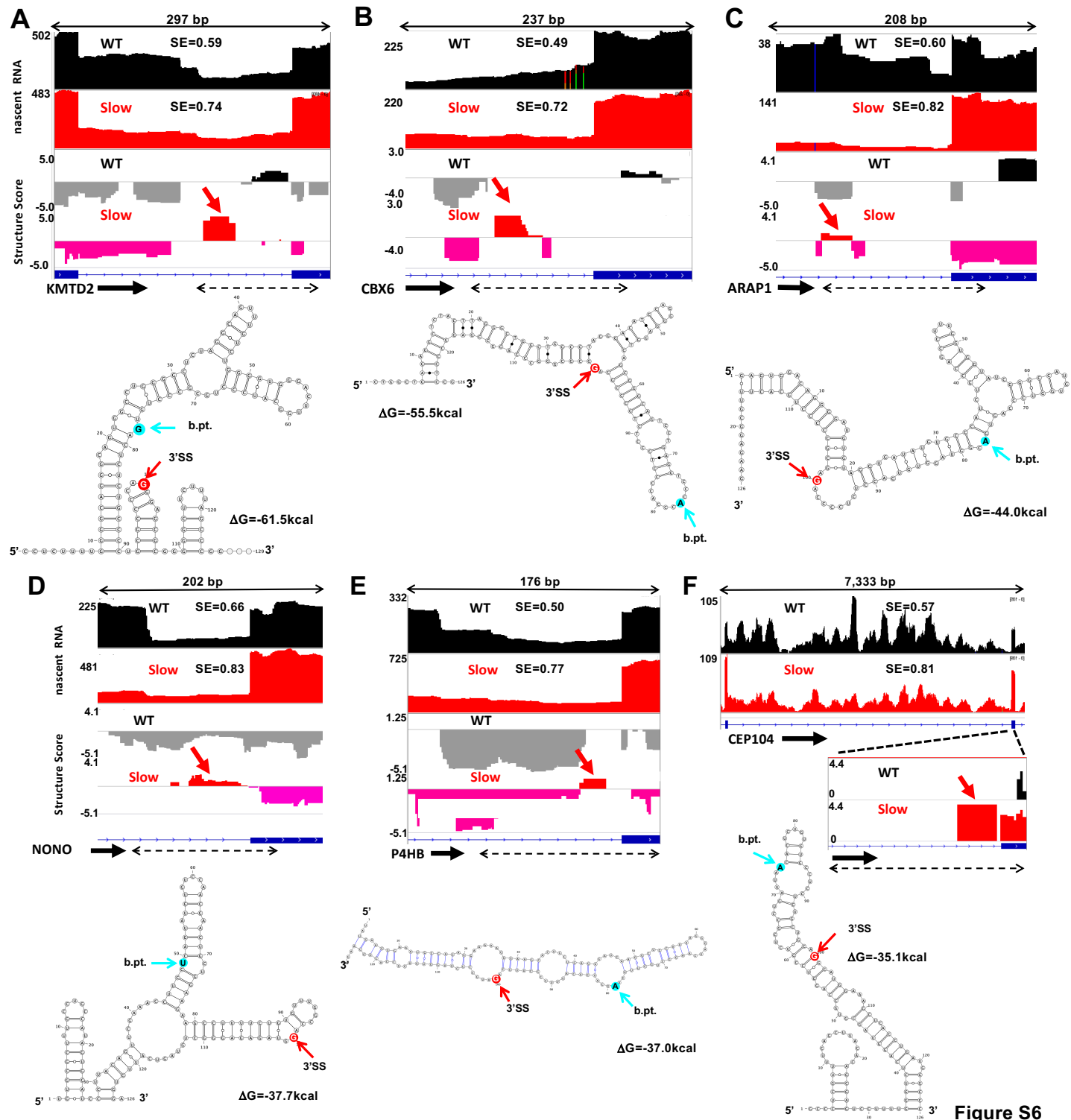
Figure S6

Figure S6. Related to Figure 5.

A-F. Elevated RNA structures (red arrows) at the 3' SS's (-100 to +30 bases) of introns with elevated co-transcriptional splicing efficiencies (SE) when transcribed by slow pol II. IGV genome browser screen shots of nascent RNA seq (tNET-seq, top panels) and Structure Scores are shown with predicted local RNA folding of regions indicated with dashed double arrows. Regions folded by RNAFold (Lorenz et al., 2011) and visualized by VARNA are (hg19) A. chr12:49436087-49436213 B. chr22:39263180-39263306 C. chr11:72404824-72404950 D.   chrX:70514147-70514273 E. chr17:79817237-79817363 F. chr1:3732908-3733034. Note RNA structures can present the indicated branch points (Pineda and Bradley, 2018) and 3' splice sites in loops or bulges.
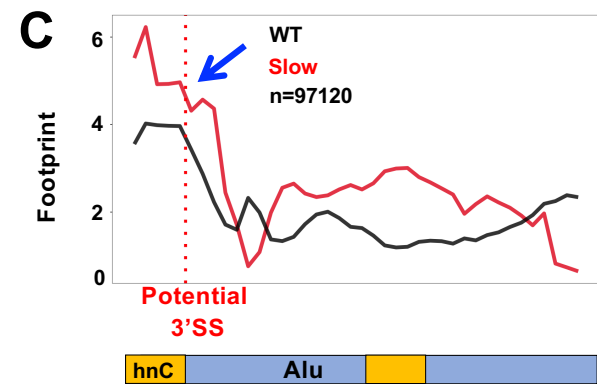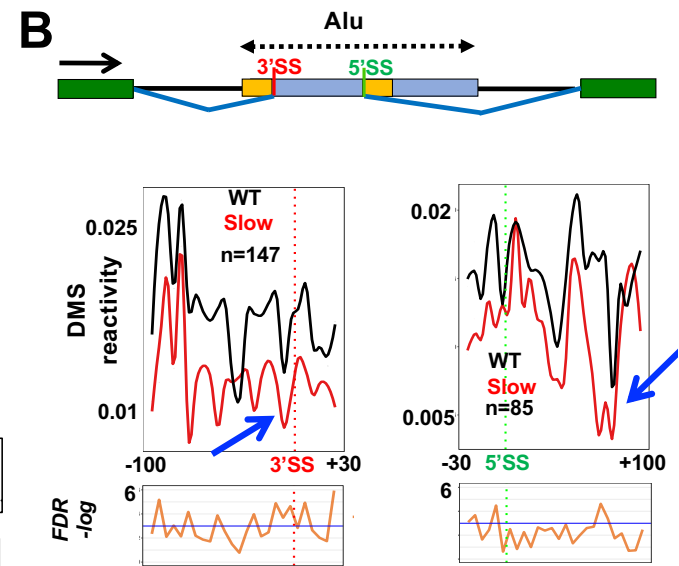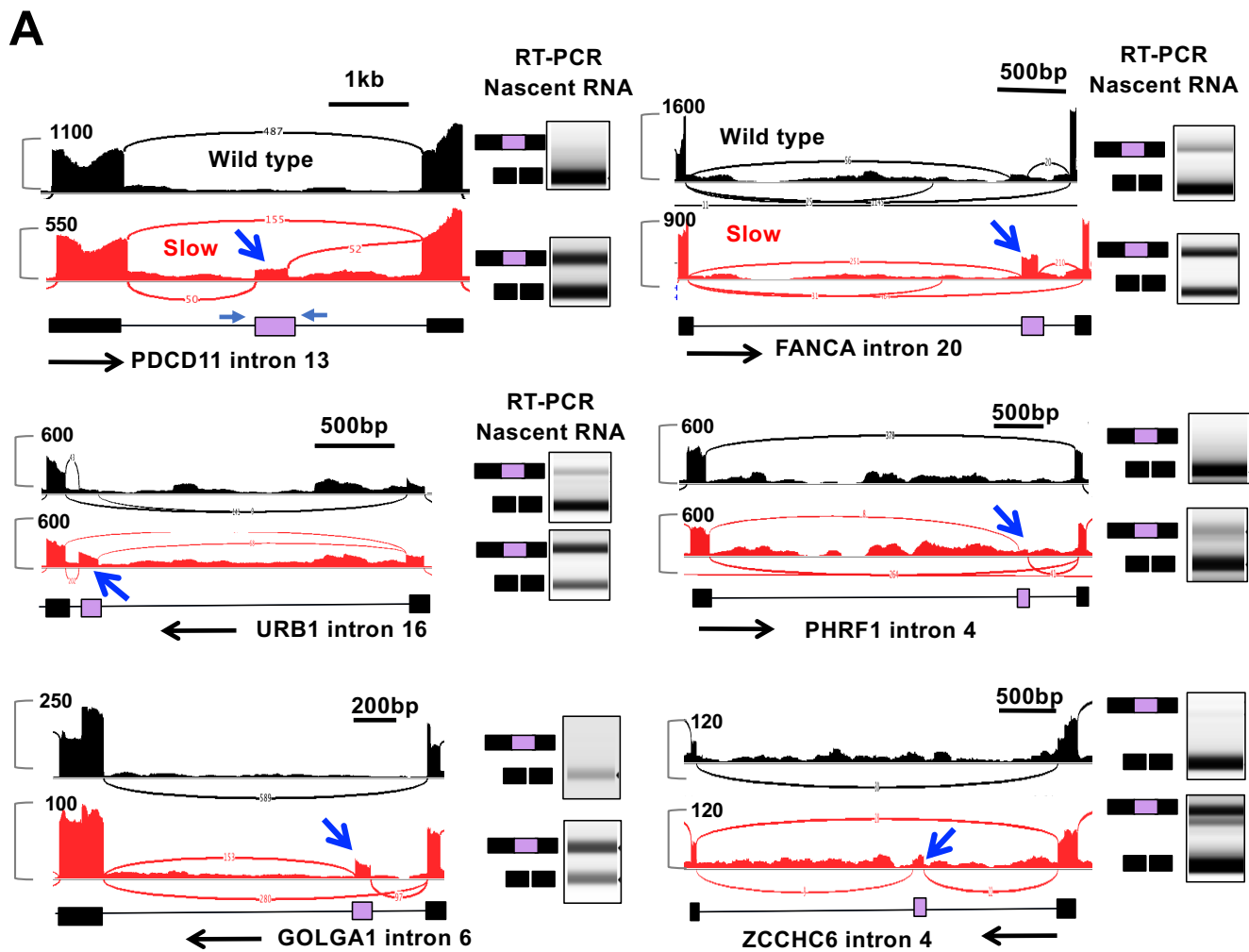
Figure S7

Figure S7. Related to Figure 6.

A. Validation of inclusion of cryptic Alu elements in nascent RNA of cells expressing slow mutant pol II (blue arrows). Left panels: Sashimi plot of nascent RNA-seq showing co-transcriptional exonization of intronic Alu's (lavender boxes) in the slow mutant. Right panels: RT-PCR confirmation on Agilent Tape Station of Alu exon inclusion in nascent RNA. Primer pairs are indicated in the first panel. Regions shown are: PDCD11 intron 13 chr10:105,176,193-105,177,798; FANCA intron 20 chr16:89,842,084-89,845,294; URB1 intron 16 chr21:33,729,833-33,732,232; PHRF1 intron 4 chr11:587,158-591,592; GOLGA1 intron 6chr9:127,683,979-127,685,535; ZCCHC6 intron 4 chr9:88,920,024-88,923,603.

B. DMS reactivity metaplots (5 base bins) across cryptic splice sites within Alu elements that become exonized in nascent RNA from cells expressing slow mutant pol II. Note increased structure (reduced reactivity, blue arrows) in the slow mutant associated with increased cryptic splice site use. Map shows antisense intronic Alu element with U rich elements (yellow boxes) and cryptic splice sites.

C. Metaplot of putative protein footprint signal from tNET-PIP-seq normalized to nascent RNA coverage across expressed (top 95%) Alu elements. U-rich elements (yellow boxes), the previously mapped hnRNPC binding site (hnC) (Zarnack et al., 2013) and the position of the commonly used cryptic 3' splice-site (red dotted line) are indicated. 40 variable length bins across Alu elements >250bp long are shown. Note slow transcription does not reduce protein footprints near the potential cryptic 3'SS in most Alu elements in contrast to those that become exonized (see Fig. 6D).
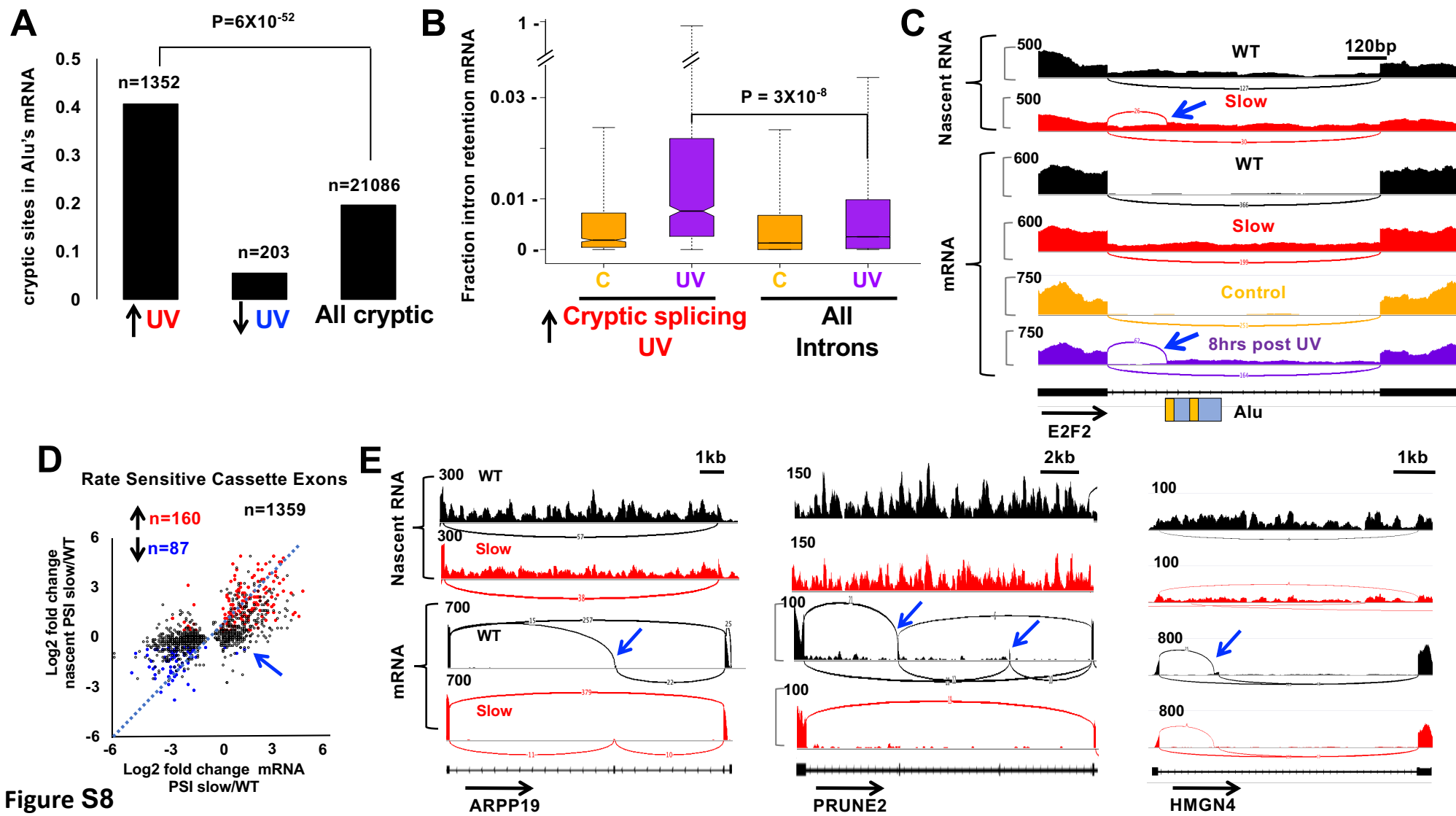
Figure S8

Figure S8. Related to Figure 6.

A. The frequency of Alu elements among cryptic 3'SS affected by UVR (See Fig. 6E). Note the high fraction of Alu's amongst cryptic exons included in response to UVR (up arrow) relative to those skipped (down arrow) or all cryptic exons. P value was calculated by Chi^2. RNA-seq data from control cells and 8 hr post UVR are from (Williamson et al., 2017).

B. Intron retention in mRNA in response to UV relative to untreated control cells (C) is enriched among introns with enhanced cryptic splicing relative to all introns. P value calculated by Chi^2.

C. IGV browser shot of cryptic splicing and intron retention (chr16:67,228,694-67,229,911) in nascent RNA of cells expressing slow pol II and in mRNA of UV irradiated cells (blue arrows).

D. Comparison of alternative splicing in mRNA and nascent RNA. Fold change in PSI in mRNA compared to nascent RNA among cassette exons affected by slow transcription in mRNA (see Fig. 5A). Red and blue circles indicate cassette exons with significant co-transcriptional changes in inclusion when transcribed by slow pol II (FDR <0.05, fold change >1.3, 3 replicates). Note that while exons with significantly changed PSI in nascent RNA correlate well with mRNA (R^2=0.64), most rate-sensitive cassette exons do not show alternative splicing changes co-transcriptionally (R^2=0.17) (black circles). Nascent RNA analysis was limited to cassette exons with ≥10% inclusion in mRNA and minimum coverage over flanking exons (see Star Methods). 658 cassette exons with altered inclusion in mRNA showed no evidence of splicing in nascent RNA and are not shown. Also see Table S8.

E. Sashimi plots of alternative cassette exon splicing in nascent RNA (top panels) and mRNA (bottom panels). Note that junctions splicing to alternative cassette exons (blue arrows) affected by slow transcription are not detectable in nascent RNA suggesting that these splices occur

predominantly post-transcriptionally. Regions shown are ARPP19 chr15:52,849,091-52,861,317;

PRUNE2 chr9:79,229,131-79,244,405; HMGN4 chr6:26,538,630-26,545,745.

Figure S9

Figure S9. Related to Figure 7.

A. Metaplots (5 base bins) of Structure Score in nascent RNA across the 5' and 3' splice sites 2 and 3 around cassette exons with altered inclusion in mRNA in the pol II slow mutant. In contrast to distal 3' splice site 4 (Fig. 7C, D), no significant structural effect of slow transcription was detected at sites 2 and 3. However consistent with the 3' SS competition model, there is detectable strengthening of the structural signature at the proximal 3' SS (site 2) specifically at exons whose inclusion is favored by slow transcription (red arrow).

B-E. Altered RNA structure (blue arrows) at the 3' SS (site 4) downstream of a cassette exon (green arrows) with enhanced skipping (B, C) or enhanced inclusion (D, E) when transcribed by slow pol II. IGV screen shots of mRNA-seq and Structure Score are shown in the region -70 to +30 bases relative to the splice site. Note that increased skipping is associated with formation of a "stronger" more structured 3'SS when transcription is slow whereas increased inclusion is associated with a "weaker" less structured 3'SS (blue arrows). B: chr7:100,877,531-100,881,040; C: chr17:48,541,629-48,548,475; D. chr17:74,731,111-74,732,442; E: chr3:156,870,823-156,876,809.